HHS Public Access

Author manuscript

ACS Nano. Author manuscript; available in PMC 2021 June 23.

Published in final edited form as:

ACS Nano. 2020 June 23; 14(6): 6649–6662. doi:10.1021/acsnano.9b09243.

Development of Optimized Tissue Factor-Targeted Peptide Amphiphile Nanofibers to Slow Non-Compressible Torso Hemorrhage

Mia K. Klein[†], **Hussein Aziz Kassam**[†], **Robert H. Lee**[Δ,¥], **Wolfgang Bergmeier**[Δ,¥], **Erica B. Peters**[†], **David C. Gillis**[†], **Brooke R. Dandurand**[†], **Jessica R. Rouan**[†], **Mark R. Karver**[ℙ], **Mark D. Struble**[ℙ], **Tristan D. Clemons**[ℙ,⊥,$], **Liam C. Palmer**[ℙ,⊥], **Brian Gavitt**[▲], **Timothy A. Pritts**[§], **Nick D. Tsihlis**[†], **Samuel I. Stupp**[ℙ,⊥,£,#,‡], **Melina R. Kibbe**[*,†,■]

[†]Department of Surgery and Center for Nanotechnology in Drug Delivery, University of North Carolina, Chapel Hill, NC, 27599, USA

[Δ]Department of Biochemistry and Biophysics, University of North Carolina, Chapel Hill, NC, 27599, USA

[¥]UNC Blood Research Center, University of North Carolina, Chapel Hill, NC, 27514, USA

[ℙ]Simpson Querrey Institute, Northwestern University, Chicago, IL, 60611, USA

[⊥]Department of Chemistry, Northwestern University, Evanston, IL, 60208, USA

[▲]United States Air Force School of Aerospace Medicine, Wright-Patterson AFB, OH, 45433, USA

[§]Department of Surgery, University of Cincinnati, Cincinnati, OH, 45267, USA

[£]Department of Materials Science and Engineering, Northwestern University, Evanston, IL, 60208, USA

[#]Department of Medicine, Northwestern University, Chicago, IL, 60611, USA

[‡]Department of Biomedical Engineering, Northwestern University, Evanston, IL, 60208, USA

[*]*Corresponding Author*: Melina R. Kibbe, MD, Department of Surgery, University of North Carolina at Chapel Hill, 4041 Burnett Womack, 101 Manning Drive, Chapel Hill, NC 27599-7050, Office: 919-445-0369, Fax: 919-966-6009, Cell: 312-203-7104, melina_kibbe@med.unc.edu.

Author Contributions

The manuscript was written through contributions of all authors. NDT, LCP, MRK1 (Karver), and MDS designed TF-targeted peptide sequences. MKK performed all conventional TEM. MKK conceived and designed the rat experiments and performed the surgeries. HAK assisted with the rat hemorrhage model. MKK and RHL conceived and designed the mouse experiments, with laser injury performed by RHL. DCG and BRD provided assistance with tissue processing and handling. MKK conceived, designed, and performed the TEG experiments. DCG provided additional assistance with TEGs. MDS and TDC performed CD spectroscopy. TDC performed cryo-TEM, SAXS, and WAXS. MRK1 synthesized all PAs. WB, EBP, LCP, NDT, TAP, SIS, MRK2 (Kibbe) helped guide the research. MKK, NDT, MRK2 interpreted all results. EBP assisted with statistical analysis. EBP and JRR performed CAC measurements. MKK prepared the initial draft of the manuscript. NDT and MRK2 critically revised the manuscript. MRK2, SIS, and BG provided oversight and funding of the entire project. All authors have given approval to the final version of the manuscript.

Supporting Information

A table of the three letter codes, amino acid sequences, and corresponding Factor VII residues for the peptides incorporated into PA molecules; crystal structure models of the putative interaction sites of the targeting peptides on TF; HPLC-MS traces showing purity of synthesized PAs; cryogenic TEM of 25% SFE and 75% SBC-2 PA nanofibers; WAXS analysis of backbone, 25% SFE, and 75% SBC-2 PA nanofibers; CD spectroscopy of FKD and TQD PA nanofibers; fluorescent quantification of tested ratios of SFE and SBC-2 PA nanofibers; the critical aggregation concentration determinations for the 75% SBC-2, 25% SFE, and backbone PAs; and real-time localization of 75% SBC-2 in a mouse laser injury model. This material is available free of charge *via* the internet at http://pubs.acs.org.

■Department of Biomedical Engineering, University of North Carolina, Chapel Hill, NC, 27599, USA

$School of Molecular Sciences, University of Western Australia, Perth, WA, 6009, Australia

Abstract

Non-compressible torso hemorrhage accounts for a significant portion of preventable trauma deaths. We report here on the development of injectable, targeted supramolecular nanotherapeutics based on peptide amphiphile (PA) molecules that are designed to target tissue factor (TF) and, therefore, selectively localize to sites of injury to slow hemorrhage. Eight TF-targeting sequences were identified, synthesized into PA molecules, co-assembled with non-targeted backbone PA at various weight percentages, and characterized *via* circular dichroism spectroscopy, transmission electron microscopy, and X-ray scattering. Following intravenous injection in a rat liver hemorrhage model, two of these PA nanofiber co-assemblies exhibited the most specific localization to the site of injury compared to controls ($p<0.05$), as quantified using immunofluorescence imaging of injured liver and uninjured organs. To determine if the nanofibers were targeting to TF *in vivo*, a mouse saphenous vein laser injury model was performed and showed that TF-targeted nanofibers co-localized with fibrin, demonstrating increased levels of nanofiber at TF-rich sites. Thromboelastograms obtained using samples of heparinized rat whole blood containing TF demonstrated that no clots were formed in the absence of TF-targeted nanofibers. Lastly, both PA nanofiber co-assemblies decreased blood loss in comparison to sham and backbone nanofiber controls by 35% to 59% ($p<0.05$). These data demonstrate an optimal TF-targeted nanofiber that localizes selectively to sites of injury and TF exposure, and, interestingly, reduces blood loss. This research represents a promising initial phase in the development of a TF-targeted injectable therapeutic to reduce preventable deaths from hemorrhage.

Graphical Abstract

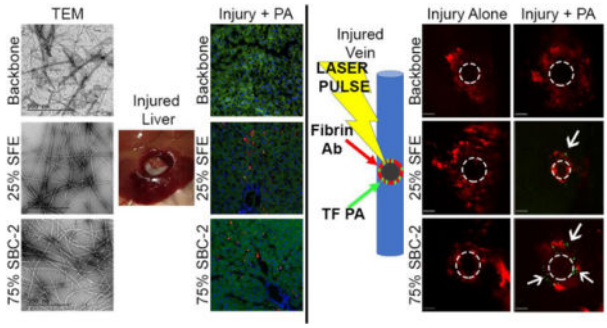

Keywords

hemorrhage; non-compressible torso hemorrhage; preventable deaths; battlefield intervention; tissue factor; nanofibers; targeted therapeutic

Hemorrhage is a leading cause of death following traumatic injury, accounting for 43% of deaths in the civilian setting and 90% in the military setting.[1, 2] Specific to the military, 67% of the potentially survivable deaths are from truncal, non-compressible hemorrhage.[2]

Current options for non-compressible torso hemorrhage are limited and not without challenges. Invasive therapies include Resuscitative Endovascular Balloon Occlusion of the Aorta (REBOA) and ResQFoam (REVIVE, NCT02880163), which both require special training by field medics, additional heavy equipment such as portable ultrasounds, and can have serious complications when inserted improperly.[3–10] Injectable therapies include tranexamic acid (TXA), which inhibits plasminogen-mediated degradation of fibrin clots.[11] However, increased rates of deep vein thrombosis in patients who receive TXA have been reported.[12] Therefore, a great need remains to develop a therapeutic to slow or stop non-compressible torso hemorrhage that is portable, lightweight, easy to administer, and highly selective for the site of injury.

Development of a targeted therapeutic that could be administered systemically through a simple intravascular route, but specifically acts only at the site of hemorrhage, would avoid off-target side effects. To develop such a therapeutic, a protein or peptide that is expressed solely at the site of injury is required. Thus, we chose tissue factor (TF) as our target. Tissue factor is present in the adventitia of all blood vessels, as well as epidermal and mucosal lining cells, but is only exposed to the blood—and therefore Factor VII (FVII)—after external damage, making it a highly selective target for the site of active hemorrhage.[13] To ultimately deliver a therapeutic agent to the site of TF exposure after injury, we chose peptide amphiphiles (PA) as the delivery vehicle. PA monomers that self-assemble into nanofibers are excellent delivery vehicles because they can be designed to deliver therapeutics either *via* encapsulation in their hydrophobic core or covalent attachment to the PA monomer. They are also easily modifiable for targeting, biocompatible, and heat- and cold-tolerant.[14, 15] In addition, the supramolecular structure of a nanofiber is ideal for intravascular applications as there is a large surface area for interaction with the site of injury, laminar flow dynamics allow for greater localization of fibers to the vascular wall compared to spheres, and fast biodegradation occurs after the therapy is delivered.[14, 16]

The overall goal of this study was to develop a PA nanofiber that targets TF with high selectivity and specificity, thereby allowing for clinical translation. We hypothesized that a PA nanofiber targeted to TF will localize in a highly selective manner only to the site of active hemorrhage.

Results/Discussion

Targeted PAs Form a Variety of Nanofibers at Different Ratios

To identify potential sequences, we reviewed literature on the interaction between TF and FVII, including both the crystal structure and mutational studies.[17–20] We chose eight targeting sequences (Supplemental Table) from different areas of FVII (Supplemental Figure 1) and used the University of North Carolina (UNC) Structural Biology Core (SBC) to modify three of those sequences to enhance α-helix formation, and therefore localization to human TF (SBC-X sequences). Of note, protein BLAST shows that the amino acid sequence of rat TF (accession number: AAA16966) is 55% identical and 66% homologous to human TF (accession number: AAA61152), and the amino acid sequence of rat FVII (accession number: AAM95967.1) is 71% identical and 81% homologous to human FVII (accession number: AAA51983.1), indicating that the results seen in rats and mice could be even better

in human patients. All eight targeting sequences (Figure 1) were synthesized and conjugated onto PA molecules and then co-assembled with backbone PA nanofiber filler (KKAAVV-K(*N*-ε-lauroyl)) at weight ratios of 25%, 50%, 75%, and 95% targeting sequence to backbone PA. Synthesized PA nanofibers were greater than 95% pure (Supplemental Figure 2). The co-assembly process is driven by the hydrophobic collapse of the lauroyl portions of the backbone and targeted PAs. Conventional transmission electron microscopy (TEM) confirmed nanofiber formation for these different PA nanofibers (Figure 2A). For *in vivo* work, 95% was used instead of 100%, as it was the highest ratio of targeting sequence that could be co-assembled and still allow for the addition of backbone PA monomers containing a fluorophore (5% by weight). Some PAs did not form nanofibers (*e.g.*, DAE, SBC-1), while some PAs formed nanofibers only at specific ratios (*e.g.*, ERT, SBC-3), and others formed nanofibers at every co-assembly ratio (*e.g.*, FKD, RTL, SBC-2, SFE, TQD). Additionally, ease of solubility in Hanks Balanced Salt Solution (HBSS) was taken into account to facilitate animal studies. RTL was included as comparison to previous work.[21]

Structure of SBC-2 and SFE PA Nanofibers

Small-angle X-ray scattering (SAXS) of non-targeted backbone nanofiber alone, 25% SFE TF-targeted nanofiber, and 75% SBC-2 TF-targeted nanofiber was used to further investigate PA structure. Analysis of scattering intensity *versus* q in the Guinier region allowed for the determination of the power law slope for each sample (backbone slope = −1.4, 25% SFE slope = −1.8, and 75% SBC-2 slope = −1.6; Figure 2B). A power slope of −1 is characteristic of cylindrical fibers, where a slope of −2 is indicative of lamellar structures. It is most probable that the PA structures fall between both of these ideal cases due to a flattened yet elongated ribbon-like structure consistent with cryo-TEM (Supplemental Figure 3A). The 25% SFE and 75% SBC-2 PAs maintained a nanofiber morphology which was seen to bundle together in the presence of 10% fetal bovine serum (Supplemental Figure 3B), indicating stability in physiologically relevant fluids. Furthermore, nanofiber aggregation and fiber-fiber interactions that enhance scattering intensity in the low q region can also add to this elevated slope and is likely the reason for the deviation of the model from the data in the low q range.[22] Fiber radii were estimated from fitting of the data with a cylindrical core-shell model, with radii increasing slightly in order of larger epitopes: backbone alone (3.6 nm), 25% SFE (3.9 nm), and 75% SBC-2 (4.3 nm). Wide-angle X-ray scattering analysis (WAXS) of backbone, 25% SFE, and 75% SBC-2 PAs shows a Bragg peak associated with β-sheet character of the fibers at q = 1.34 A^{-1} (Supplemental Figure 4). This peak is considerably reduced in the 75% SBC-2 sample compared to the backbone and 25% SFE and qualitatively shows that β-sheet contributions are involved in the fiber structure formation.

SBC-2 and SFE PA Nanofibers Display Alpha-Helical Structures

The secondary structure of the TF-targeted PA nanofibers was assessed by circular dichroism (CD) spectroscopy (Figure 2C). The CD spectra of the SFE-PAs at all weight ratios, but most pronounced at 95% and 100%, showed a positive band at 193 nm and minima at 206 and 216 nm. This is consistent with a mixture of α-helical character (positive band at 193 nm and first minima at 206 nm) seen in the structure of the peptide sequence in FVII[17] and β-sheet-like character (positive band at 193 nm and second minima at 216 nm)

from the PA assembly.[23, 24] The data also suggest minimal contributions of random coil interactions due to no negative band present below 200 nm and significant ellipticity measured above 210 nm.[25]

The epitope of the SBC-2 PA nanofiber was designed to have enhanced α-helical character. CD spectra of the SBC-2 PA showed a positive band at approximately 193 nm and minima at 207 nm and 217 nm. These peak positions are consistent with a mixture of α-helical character (positive band at 193 nm and first minima at 207 nm) from the SBC-2 sequence and β-sheet-like character (positive band at 193 nm and second minima at 217 nm) from the PA assembly.[23, 24] Again, minimal contributions of random coil interactions were observed due to no negative band present below 200 nm and significant ellipticity measured above 210 nm.[25] The contribution of β-sheet was further confirmed by WAXS analysis (Supplemental Figure 4).

TF-Targeted Nanofibers Localize to Areas of Liver Injury *In Vivo*

To determine if the TF-targeted nanofibers localize to the site of hemorrhage using a non-compressible torso injury model, rats underwent central liver punch injury and blinded intravenous injection of the TF-targeted nanofibers, control backbone PA nanofibers, or HBSS (sham). TF-targeted PAs that formed nanofibers at all co-assembly ratios were evaluated using this animal model (*i.e.*, FKD, SBC-2, SFE, and TQD PAs at 25, 50, 75, and 95% targeting sequence ratios). Localization of the TF-targeted nanofibers to the site of injury was assessed and quantified using standard fluorescence microscopy imaging of the liver (Figure 3). While FKD and TQD PAs did form nanofibers (as shown by TEM in Figure 2A and CD spectroscopy in Supplemental Figure 5), in a non-compressible hemorrhage model these nanofibers increased blood loss compared to sham animals, impaired clot formation, and were associated with ischemic events at the tail vein injection site, ultimately resulting in animal mortality. Therefore, additional testing on those PAs was aborted early.

25% SFE PA and 75% SBC-2 PA nanofibers were well-tolerated by the animals and had the highest average amount of fluorescence observed at the site of liver injury when compared to other co-assembly ratios tested (Supplemental Figure 6). Although SBC-2 PA had higher fluorescence than SFE PA, the most successful ratio of each PA was chosen for additional testing, as these targeting sequences interact with different areas on TF. The critical aggregation concentrations of 25% SFE PA, 75% SBC-2 PA, and backbone PA were found to be 5.5 ± 1.1, 7.8 ± 1.9, and 4.8 ± 1.0 μM, respectively (Supplemental Figure 7). These values are all well below the final concentration of the injected dose when diluted in the blood volume (~20 mL for a 300 g rat, or 93, 55, and 106 μM, respectively), suggesting that these PAs remained co-assembled as nanofibers upon injection in the rats. No significant difference in fluorescence was seen in the injured *versus* uninjured livers of rats that were treated with backbone PA nanofiber ($p = 0.9372$, Figure 3B). Quantification of the fluorescence in the liver sections confirmed that the 25% SFE PA nanofiber and 75% SBC-2 PA nanofiber had significantly higher fluorescence in the injured lobe of the liver compared to the uninjured lobe of the liver (Figure 3B, $^*p < 0.05$), with 75% SBC-2 PA nanofiber demonstrating nearly twofold greater localization than 25% SFE PA nanofiber (Figure 3B, $\$p < 0.05$). Additionally, fluorescence was greater in injured livers in 25% SFE PA and 75%

SBC-2 PA nanofiber treatment groups compared to injured livers from rats that received the backbone PA nanofiber (Figure 3B, #p < 0.05). Sham animals had no fluorescence in injured or uninjured livers at the thresholds used. These data suggest that the 25% SFE PA nanofiber and 75% SBC-2 PA nanofiber localize selectively to the site of liver injury.

TF-Targeted Nanofibers Do Not Localize to Uninjured Organs *In Vivo*

To further evaluate specificity of the TF-targeted PA nanofibers, sections of lung, spleen, and kidney from animals injected with 25% SFE and 75% SBC-2 PA nanofibers were imaged and the fluorescence was quantified using standard fluorescence microscopy (Figure 4). Sham animals had no fluorescence in any organs at thresholds examined. After blinded injection of the fluorescently labeled nanofibers and liver injury, there was no difference in fluorescence between backbone PA nanofiber, 25% SFE PA nanofiber, and 75% SBC-2 PA nanofiber in lung, spleen, or kidney (Figure 4B, p = N.S.). Minimal fluorescence was noted in other organs compared to injured liver in TF-targeted PA nanofiber treatment groups. These data suggest that the SFE and SBC-2 TF-targeted PA nanofibers localize specifically to the site of injury and not to uninjured, off-target sites. Previous studies have shown that similar PAs are metabolized by the liver and excreted through the kidneys, without long-term adverse effects on coagulation factors or liver enzymes.[26]

SFE and SBC-2 PA Nanofibers Decrease Blood Loss

Next, we evaluated the ability of the SFE and SBC-2 TF-targeted nanofibers to decrease blood loss (Figure 5A) in our rat central liver punch injury model (Figure 5A, inset) of non-compressible hemorrhage. Surprisingly, with a TF-targeting sequence alone and no therapeutic agent incorporated, both 25% SFE and 75% SBC-2 PA nanofibers decreased blood loss compared to sham treated animals (Figure 5A, *p < 0.05). 25% SFE and 75% SBC-2 PA nanofibers also decreased blood loss compared to backbone PA nanofiber control (Figure 5A, #p < 0.05). Specifically, 75% SBC-2 PA nanofibers decreased blood loss by 59% compared to sham and backbone PA nanofiber treatment groups (9 ± 2.2% *versus* 21.4% ± 1.5 and 21.8% ± 2.7, respectively) while 25% SFE PA decreased blood loss by 35% compared to sham and backbone PA nanofiber treatment groups (15 ± 1.4% total blood loss).

The impact on blood loss without incorporation of a therapeutic into the TF-targeted nanofiber was surprising to us. One possible explanation is that the lysine residues in our KKAAVV PA backbone nanofiber themselves have an antifibrinolytic function.[27] If this is the case, the TF-targeting sequence could allow more of the targeted nanofiber containing the lysine-loaded backbone to accumulate at the injury site, which could be affecting fibrinolysis. We have also previously published data showing that platelets adhere to surfaces coated with TF-targeting PAs and that TF-targeting PAs reduce fibrinogen in whole blood,[21] indicating that the structures of our nanofibers may potentiate additional fibrin clot formation. These data suggest that TF-targeted PA nanofibers without incorporation of a therapeutic have some intrinsic properties to reduce hemorrhage.

TF-Targeted Nanofibers Facilitate Clot Formation in Rat Blood

To determine the effect on clotting with PA nanofibers, rats underwent terminal cardiac puncture for blood withdrawal into a syringe containing heparin (10 units/mL) and evaluation by thromboelastography. This technique measures the ability of blood to coagulate around a thin wire probe, allowing for determination of several values to determine clot strength: R time (reaction time) measures the speed of clot formation, K time (kinetic time) measures the speed with which a clot reaches a specific strength, MA (maximum amplitude) indicates the highest strength the clot achieves, and LY30 (lysis 30 minutes after MA) measures the stability of the clot. Taken together, these values provide insight into the activity of coagulation factors in the blood sample. Heparin was used as an anti-coagulant because rats are more prone to coagulation at baseline and we were unable to determine treatment effect without anti-coagulation of the sample, as clotting occurred too rapidly.[28] Citrate was not used as an anti-coagulant as studies looking at TF-dependent reactions are impaired by citrate chelation.[29] Furthermore, the high levels of calcium required to overcome citrate chelation can negatively affect nanofiber formation.

No clotting was observed at 60 minutes in TF-activated blood treated with HBSS (sham) or backbone PA nanofiber (Figure 5B). Clotting was seen in TF-activated blood treated with 25% SFE PA nanofiber or 75% SBC-2 PA nanofiber, with no significant differences seen in R time, K time, MA, or angle between the TF-targeted PA nanofibers (Figure 5C). No clotting was seen in any group, including TF-targeted PA nanofibers, when coagulation was not initiated with TF. Taken together, these data suggest that our TF-targeted PA nanofibers are dependent upon TF to initiate clotting, and are facilitating clot formation despite the anti-coagulation caused by heparin. This is interesting, as the PAs were designed only to target TF, not to have a therapeutic effect. Of note, TEG assays were run for up to 2 hours without any clot lysis observed, and our *in vivo* model was carried out for 30 minutes, indicating that the TF-targeting PAs may be acting to decrease blood loss by preventing clot lysis.

TF-Targeted Nanofibers Co-Localize with Fibrin *In Vivo*

To determine if the targeted PA nanofibers localize to sites where TF is expressed, mice were subjected to a vascular laser injury model and enrichment at the site of injury was assessed in real time using epifluorescence and spinning disk confocal microscopy. Co-localization with fibrin, the product of TF/thrombin activity,[30] was assessed using AF488-labeled PA nanofibers and AF647-labeled fibrin antibody. Fluorescently labeled fibrin antibody was used instead of TF antibody to prevent interference with nanofiber targeting to TF.

No localization was observed at the site of injury nor was any co-localization with fibrin observed in animals treated with backbone PA nanofiber (Figure 6A). Some localization (green fluorescence) at the site of injury was seen with 25% SFE PA nanofibers, which co-localized within the fibrin ring (red fluorescence, Figure 6A). Extensive localization at the site of injury within the fibrin ring was seen with 75% SBC-2 PA nanofibers, largely occurring where TF is exposed (Figure 6A, white arrows). Orientation of the mouse leg for laser injury can be seen in Figure 6B. Epifluorescence videos of real time localization of 75% SBC-2 PA nanofibers immediately after laser injury can be seen in the Supplemental

Video. A 3D reconstruction of the clot Z-stacks showing the localization of the 75% SBC-2 PA fluorescence (green) in the red fibrin ring is included as Supplemental Figure 8.

Despite the 75% SBC-2 PA nanofiber having a lower percent of backbone PA nanofiber (25%), we have demonstrated that it is superior to the SFE PA nanofiber (containing 75% backbone PA nanofiber) in terms of localization in multiple animal models, which we believe could be overcoming the lower amount of lysine residues present in the backbone. Backbone PA nanofiber control contains no sequence targeting it to the site of injury, which may be why it has no effect on blood loss or localization to TF in the laser injury model. These data suggest that our TF-targeted nanofibers are specifically localizing to the site of TF exposure, with the 75% SBC-2 PA nanofiber showing superior localization compared to the 25% SFE PA nanofiber.

Comparison to Previous Studies

The current study significantly builds upon our previously published TF-targeting sequence (RTL).[21] First, we improved upon selectivity to the site of injury with the synthesis and thorough evaluation of eight additional TF-targeting PA nanofibers.[21] Additionally, we improved upon RTL by modifying three of these sequences to enhance localization to human TF using a rigorous structural biology approach. Second, we eliminated bias that may have existed with our previous studies by blinding the surgeon to the injection. Third, we performed quantification of fluorescence on all collected organs (lung, liver, kidney, and spleen) to more thoroughly evaluate non-specific off-target localization. Fourth, we showed strong evidence that our TF-targeted nanofibers bound to TF by demonstrating that they localized to TF-rich areas using the mouse laser injury model and real time epifluorescence microscopy. To ultimately translate our work to the clinical arena, we need to develop a targeted nanotherapeutic that localizes to the site of injury and nowhere else. Therefore, the current study significantly advances our prior work and is necessary in order to proceed with incorporation and evaluation of a therapeutic into the TF-targeted nanofiber.

Comparison of TF-Targeted PAs to Current Therapies

Several injectable therapeutics currently under investigation deserve mention. Two therapies, RGDS nanospheres and Synthoplate, target platelets. While promising, these therapies were shown to have very narrow therapeutic windows and exhibited accumulation in uninjured organs.[31–36] We have not determined a therapeutic dosing window for our TF-targeted nanofibers as we have not yet incorporated a therapeutic agent. However, research with other targeted PA nanofibers tested with a range of doses and concentrations demonstrated safety with 5 mg dosing in similar sized rats (double our current dose).[26] Another therapeutic under investigation is polySTAT, a synthetic polymer that stabilizes the fibrin clot by crosslinking fibrin monomers. Unfortunately, polySTAT was shown to remain in the kidney 1 week after injection.[37] Our PA nanofibers have a relatively short half-life, making them an ideal candidate to augment clotting.[21] Once a clot is formed and bleeding stops, the risk-benefit ratio of having the therapeutic present in the circulation rises significantly. Therefore, an intravascular targeted therapeutic to slow non-compressible hemorrhage should have a short half-life. Lastly, investigators have evaluated the benefits of a bolus administration of adenosine, lidocaine, magnesium (ALM) followed by continuous infusion. This therapy is

designed to slow blood loss and improve mortality by correcting early defects in coagulation and preventing fibrin degradation.[38, 39] A challenge with this therapy is that it is not easily deployed in the field, as field medics and/or soldiers would not be able to carry enough ALM for this administration scheme, and establishing a continuous infusion would be challenging. In contrast, our TF-targeted nanofiber can be carried on the person in a very small vial that simply needs to be reconstituted with saline and injected.

Limitations

First, this study was designed to provide the highest likelihood of localization of the TF-targeted PA nanofiber to TF. Previous work in our lab with a different TF-targeted PA nanofiber demonstrated that 70% remained in plasma at 30 minutes.[21] Hence, for this study, the PA nanofibers were injected immediately before injury in both animal models to ensure the highest amount of nanofiber was in circulation. Once a therapeutic agent is incorporated into the PA nanofiber, we will assess the impact of injection timing (pre- and post-injury) on both localization and bleeding. Safety, dose, and duration studies will also be performed once a therapeutic agent is incorporated. Those studies were not done in this initial targeting phase, as the addition of a therapeutic will likely affect these parameters, but studies to assess these parameters are currently underway in the lab. Studies done with similar PAs did not show long-term effects of PAs on liver enzymes or tissue architecture.[26] Second, while we tried various methods including surface plasmon resonance (SPR) and biolayer interferometry (BLI), we were not able to determine binding constants of the peptide epitopes/PAs for TF. This inability to observe binding with these methods may be due to an affinity that is too low to detect by SPR or BLI. Third, the amount of PA in uninjured organs was only assessed 30 minutes after injury. Future studies will assess longer time points in both injured and non-injured organs, as well as efficacy in an animal with multiple injuries to simulate the typical polytrauma patient. Similarly, survival over longer time points will need to be assessed, in addition to the effect of repeat dosing. Fourth, we did not assess PA localization in the brain, as it is unlikely that the PAs crossed the blood-brain barrier; however, we are planning to confirm this in future studies. Fifth, we did not perform TEGs on FKD and TQD PAs, due to the issues observed in the animals we tested. Future studies will test these PAs co-assembled with a therapeutic PA *in vitro* and *in vivo*, as addition of the therapeutic PA will change many parameters.

Conclusions

In conclusion, we synthesized and screened multiple different TF-targeted PA nanofibers to determine the targeting sequence that results in the most sensitive and specific localization of the targeted nanofiber to the site of liver injury following intravascular administration. While some of the TF-targeted PA nanofibers appeared to prevent normal coagulation (FKD, TQD), the SFE and SBC-2 PA nanofibers not only localized to the site of injury and TF expression, they also decreased blood loss. Additionally, we have demonstrated efficacy of selective targeting in both a compressible and non-compressible small animal hemorrhage model and shown that these TF-targeted PA nanofibers localize to TF-rich areas. These data represent the initial phase of the development of an injectable, targeted therapeutic to slow or stop hemorrhage. After incorporation of a therapeutic and further pharmacokinetic and

pharmacodynamic studies, this treatment has the capability to decrease or even eliminate potentially preventable deaths from hemorrhage after trauma.

Methods/Experimental

Study Design

The purpose of this study was to test the hypothesis that our TF-targeted nanofibers localize to TF and, therefore, the site of injury. This targeting phase will allow for later incorporation of a therapeutic agent into the nanofiber, to ultimately slow non-compressible torso hemorrhage. After identification of potential TF-targeting sequences, they were synthesized into peptide amphiphiles and screened with conventional TEM for nanofiber formation. Sequences forming the best fibers were tested further (cryogenic TEM, circular dichroism spectroscopy, small-angle X-ray scattering, and wide-angle X-ray scattering). For animal work, two different control groups were used for all studies: sham (HBSS) and non-targeted backbone nanofiber control, and two different treatment groups were used: 25% SFE and 75% SBC-2. Targeted nanofibers were tested at multiple different co-assembly ratios in our rat non-compressible hemorrhage model; n=6 per group unless testing was stopped early due to animal deaths (minimum detectable difference in means 0.21, power 0.8, alpha 0.05). Testing was stopped early (before n=6) if animals had higher blood loss than sham, died before the 30-minute time point, or developed thrombotic complications. For the non-compressible hemorrhage model, animals were randomly assigned to treatment or control, and the surgeon (MKK) was blinded to the injection type received by the animal (given by HAK). For TEGs, the controls were as stated above, and treatment groups were 25% SFE and 75% SBC-2 TF-targeted nanofibers. Animals were randomly assigned to treatment groups, each 1 mL blood sample was treated in duplicate for n=6 (minimum detectable difference in means 0.5, power 0.8, alpha 0.05). More animals than determined by the power calculation were used to account for animal-to-animal variability. Confocal microscopy experiments were done on randomly assigned mice for n=3/group (minimum detectable difference in means 0.5, power 0.8, alpha 0.05). Groups were the same as described in rat work. Multiple injuries were able to be visualized in the same mouse, since this is known not to cause a hypercoagulable state in the mouse;[30] therefore, fewer animals were used.

The study protocol was reviewed and approved by the University of North Carolina – Chapel Hill Institutional Animal Care and Use Committee and the Air Force Medical Services Agency Office of Research Oversight and Compliance. Animals were handled and studies were conducted under a program of animal care accredited by the Association for Assessment and Accreditation of Laboratory Animal Care International and in accordance with the National Research Council's *2011 Guide for the Care and Use of Laboratory Animals* (in compliance with Department of Defense Instruction 3216.1).

Peptide Synthesis

Unless otherwise noted, all reagents are from Sigma-Aldrich (St. Louis, MO), and all amino acids are from P3 Biosystems (Louisville, KY). Peptide amphiphile (PA) molecules were synthesized *via* standard 9-fluorenyl methoxycarbonyl (Fmoc) solid-phase peptide chemistry on Rink amide MBHA resin using a CEM Liberty Blue automated microwave peptide

synthesizer (CEM Corp.; Matthews, NC). Manual loading of Fmoc-Lys(4-methyltrityl) and lauric acid were performed as previously described.[21] Automated coupling reactions were performed using 4 equivalents (eq.) Fmoc-protected amino acid, 4 eq. of *N,N'*-diisopropylcarbodiimide (DIC), and 4 eq. ethyl(hydroxyimino)cyanoacetate (Oxyma pure). Removal of the Fmoc groups was achieved with 20% 4-methylpiperidine in DMF. Peptides were cleaved from the resin using standard solutions of 95% TFA, 2.5% water, 2.5% triisopropylsilane (TIPS) (cysteine-containing peptides included 3% 2,2′-(Ethylenedioxy)diethanethiol (DODT) and 92% TFA with the same TIPS/ H_2O mixture), precipitated with cold ether, and then purified by reverse-phase HPLC on a Prep150 (Waters Corp.; Millford, MA) or Prominence (Shimadzu Scientific Instruments; Columbia, MD) HPLC using a water/acetonitrile (each containing 0.1% v/v trifluoroacetic acid or 0.1% NH_4OH) gradient. Eluting fractions containing the desired peptide were confirmed by mass spectrometry using a 6520 QTOF LCMS (Agilent; Santa Clara, CA). Confirmed fractions were pooled and the acetonitrile was removed by rotary evaporation before freezing and lyophilization. Purity of lyophilized products was tested by LCMS.

For PAs labeled with 5-carboxytetramethyrhodamine (TAMRA), the dye was coupled directly to the N-terminal amine of the PA using 1.2 eq. of TAMRA, 1.2 eq. of PyBOP (benzotriazol-1-yl-oxytripyrrolidinophosphonium hexafluorophosphate), and 8 eq. of *N,N*-diisopropylethylamine (DIEA) for approximately 18 hours. For PAs labeled with Alexa Fluor™ 488, 4 molar eq. of the purified cysteine-containing PA was dissolved with Alexa Fluor™ 488 C5 Maleimide in DMF. The progress of the reaction was monitored by mass spectrometry until consumption of the dye peak was complete (approximately 3 hours) and the dye labeled conjugate was then separated from unreacted PA by HPLC. The cyclic PA SBC-1 was formed by dissolving the purified linear PA in basic water (approximate pH 9 with NH_4OH) at a concentration of 0.75 mg/mL before adding H_2O_2 to a final concentration of 0.05%. The cyclized product was seen within 10 minutes by mass spectrometry (GSC*LPAFEGRNC*ETHKDDQL-G-KKAAVV-K(*N*-ε-lauroyl)-K(C_{12})), which was then purified by HPLC (C* indicates a cysteine involved in a disulfide bond).

PA co-assemblies were prepared by dissolving each individual PA in 1,1,1,3,3,3-hexafluoro-2-propanol (HFIP) at 2 mg/mL. After mixing the PAs in the appropriate ratios, the solutions were horn sonicated for five 10-second intervals, frozen in liquid nitrogen, and placed under high vacuum until dry. The resulting materials were then reconstituted in ultrapure water, frozen with liquid nitrogen, and lyophilized to dryness.

Conventional Transmission Electron Microscopy

Conventional TEM images were taken on a FEI Tecnai T-12 TEM (ThermoFisher Scientific; Hillsboro, OR) at 80 kV with an Orius® 2k × 2k CCD camera (Gatan, Inc.; Pleasanton, CA). PAs at 0.5 mg/mL in HBSS were prepared for TEM by negative staining. Briefly, 8 μL samples were incubated onto 400-mesh copper grids covered with a thin carbon film and previously treated with glow discharge. After three minutes, samples were stained with 2% uranyl acetate for 2–3 minutes and air-dried before imaging.

X-ray Characterization

X-ray characterization of the PAs was performed at the advanced photon source in the Argonne National Laboratory on beamline 5-ID-D, DuPont-Northwestern-Dow Collaborative Access Team Synchrotron Research Center. Samples were prepared at 0.5 wt % in HBSS solution. X-ray energy of 17 keV was selected using a double-crystal monochromator. Data was collected simultaneously across three Rayonix detectors, model numbers SAXS – LX170HS, MAXS - LX170HS, WAXS – MX170HS. For studies of the PAs in solution, samples were oscillated with a syringe pump during exposure to prevent beam damage and obtain more uniform data. Scattering patterns of samples containing 1X HBSS alone as well as the empty capillary were also collected to perform background subtractions. No attempt was made to convert the data to an absolute scale. The plots of scattering intensity *versus* q were obtained using Igor Pro v7 and the resulting plots were fitted to a core-shell cylinder model with Irena.[40]

Circular Dichroism (CD) Spectroscopy

CD measurements were performed at a concentration of 1 mM in HBSS using a Jasco J-815 CD spectrophotometer (Jasco Analytic Instruments; Easton, MD) at 25°C using a 0.1-mm path length demountable quartz cuvette. The far-UV spectral region (190–250 nm) was observed to determine if the assemblies contained secondary structure. Background subtraction of the HBSS buffer was performed. The data is an average of two scans. Data points were taken every 0.2 nm with an analysis time per data point of 120 milliseconds.

Rat Liver Punch Injury Model

To evaluate localization to the site of non-compressible torso hemorrhage and examine if there was an effect on bleeding, TF-targeted nanofibers were evaluated in a rat liver punch injury model. Adult male Sprague-Dawley rats weighing 250–300 g were anesthetized using inhaled isoflurane (1–5%). They underwent invasive hemodynamic monitoring *via* common carotid artery cannulation, as previously described.[41] PA solutions were prepared by dissolving 2.5 mg of PA in 1 mL of HBSS for a final concentration of 2.5 mg/mL. Rats were then prepared and draped in a sterile fashion. A midline laparotomy was performed, and the left lateral lobe of the liver was exposed. The animal then received tail vein injection with either sham (HBSS) or PA nanofiber solution (TF-targeted PA nanofibers or backbone PA nanofibers alone). This dose (2.5 mg) was chosen based on prior work demonstrating localization of targeted PAs to the injured liver, and their ability to be tolerated by the rat.[21] The primary surgeon (MKK) was blinded to the treatment group administered to the rat as a second surgeon (HAK) performed all tail vein injections. Immediately after injection, a 12-mm punch was created in a central location in the left lateral lobe to induce hemorrhage. The liver bled freely into the abdominal cavity over a period of 30 minutes. Shed blood was collected with pre-weighed gauze every 2 minutes for the first 10 minutes and every 5 minutes thereafter, as previously described.[21] Mean arterial pressure was monitored at the same time points when shed blood was collected. At the end of 30 minutes, the animals were euthanized. There were n=6 animals per treatment group.

Tissue Processing

In situ perfusion with 250 mL of PBS solution was performed after euthanasia *via* bilateral thoracotomies. Organs including injured liver, uninjured liver (inferior right lobe), punch biopsy liver, kidney, spleen, and lung were collected for tissue processing. Samples were fixed with 2% paraformaldehyde for 2 hours followed by 30% sucrose overnight. Samples were then frozen in Tissue-Tec OCT compound (Sakura Finetek; Torrance, CA) over liquid nitrogen and stored at −80°C until sectioning. A CryoStar NX70 (ThermoScientific) cryostat was used to cut samples into 7-μm sections, which were stained and fixed with Prolong Gold antifade reagent (Life Technologies; Eugene, OR) containing 4’,6-diamidino-2-phenylindole (DAPI).

Fluorescence Microscopy

Digital images were acquired using a Zeiss Axio Imager.A2 microscope (Hallbergmoos, Germany) with a 20X objective. The HE CY3 filter (Zeiss filter #43) using excitation and emission wavelengths of 550–575 and 605–670 nm, respectively, was used to assess TAMRA labeled PA fluorescence. The DAPI filter (Zeiss filter #49) was used for nuclear staining using excitation and emission wavelengths of 365–395 and 445–450 nm, respectively. The green fluorescent protein filter (Zeiss filter #38) using excitation and emission wavelengths of 470–495 and 525–550 nm, respectively, was used to assess tissue autofluorescence of tissues.

For quantification of the amount of fluorescence in injured and uninjured livers, as well as lungs, spleens, and kidneys, the HE CY3 filter was used to image the tissue at 20X magnification. Images were taken at each of the 4 quadrants on the slide, with exposure times adjusted to eliminate any background autofluorescence of the tissue and therefore only image the PA. Images were taken on 4 different slides evenly spaced throughout the tissue. Area of fluorescence, expressed in relative fluorescence units (RFUs) was generated using ImageJ software, and thresholds were set to only visualize the PA. Sham animals were imaged and quantified to eliminate all tissue autofluorescence, making the RFUs for all sham animals zero. Comparisons of RFUs were made between TF-targeted PA nanofibers and backbone PA nanofibers.

Thromboelastography (TEG)

TEG measurements were performed with a TEG-5000 Thromboelastograph Hemostasis Analyzer (Haemoscope Corporation; Niles, IL). Blood draws were performed by terminal cardiac puncture in male Sprague Dawley rats, with the first 500 μL of blood withdrawn discarded. Subsequent blood draws were performed using 1 mL syringes each containing 10 units of heparin, with approximately 2–4 mL of blood withdrawn from each animal. Clotting was initiated by adding Dade® Innovin® human TF (Siemens, Marburg, Germany) in a 1:200,000 dilution to whole blood. The sample was gently inverted, and then either control (HBSS or Non-targeted backbone nanofiber) or treatment nanofibers (25% SFE or 75% SBC-2) were added (0.2 μg nanofiber dissolved in 100 μL HBSS or 100 μL HBSS alone). The mixture (360 μL) was then transferred to the TEG chamber. Each 1 mL of blood was run in duplicates to ensure reproducibility. As 2–4 mL of blood were taken from each animal, multiple different treatments were performed on blood collected from the same

animal to account for animal-to-animal variability in clotting. Measurements were performed for a minimum of 1 hour at 37°C, up to 2 hours in some cases, and relevant parameters were extracted from the curve generated. Additional experiments were performed in parallel with and without addition of TF to the same sample of blood to determine if TF was required for clotting with the TF-targeted nanofibers.

Mouse Saphenous Vein Laser Injury Model

To evaluate co-localization of the TF-targeted PA nanofibers to the site of TF expression in real time, the saphenous vein laser injury model was performed in mice as previously described with some modifications.[30] Adult female wild type C57BL6 mice weighing 20–23 g were anesthetized using inhaled isoflurane (2%). A tail vein catheter was placed using 29½ gauge insulin needles placed inside 2 French tubing and secured in place with glue (LiquiVet Rapid Tissue Adhesive). The left leg was then prepped in a sterile fashion. Skin and any tissue overlying the saphenous vein was dissected free to allow visualization of the vein. Anti-fibrin antibody (generously provided by Rodney Camire) labeled with Alexa Fluor™ 647 was injected at a dose of 2.5 μg/mouse before the mouse was placed under the microscope. Injury to the endothelium (~50 μm) was initiated using an Ablate! Photoablation system equipped with an attenuable 532 nm pulse laser (Intelligent Imaging Innovations; Denver, CO) and fluorescence intensity was recorded. Following initial control injury with fibrin antibody alone, PA (TF-targeted nanofiber or backbone PA nanofiber) was administered *via* tail vein catheter and a second injury was made and recorded. PA solutions were prepared by dissolving 8 mg/kg of PA in 100 μL HBSS. Wide field epifluorescence videos were recorded for 2–3 minutes following laser ablation at each injury site with a Zeiss Axio Examiner Z1 microscope (Intelligent Imaging Innovations) equipped with a multicolor LED light source (Lumencor; Beaverton, OR) and an Orca Flash 4.0 camera (Hamamatsu Corp.; Bridgewater, NJ). After sacrificing the mouse by isoflurane overdose, spinning disk confocal (Yokogawa CSU-W1; Musashino, Japan) Z-stacks were collected at each injury site with 488 and 647 lasers (Intelligent Imaging Innovations). Representative max Z projections of spinning disk confocal Z-stacks for pre- and post-PA injury sites are shown for n=3 animals per treatment group.

Statistics

Quantification data are presented as area of fluorescence, in RFUs, which was the average from 16 images per tissue (4 images per slide; 4 slides per animal). Results were expressed as mean ± the standard error of the mean (SEM). JMP (SAS Institute, Inc.; Cary, NC) was used to determine differences between injured and uninjured livers using a two-way analysis of variance (ANOVA) followed by a Tukey Honest Significant Difference post-hoc test. Blood loss data are presented as % total blood volume, as previously described.[41] Results were expressed as mean blood loss ± SEM. JMP was used to determine differences between groups using one-way ANOVA followed by a Student’s t-test.

Supplementary Material

Refer to Web version on PubMed Central for supplementary material.

Acknowledgments

This study was supported, in part, by funding from the Department of Defense AFRL/RQKHC (FA8650-16-2-6G19 to BG, MRK2, TAP, and SIS), the National Institutes of Health (1R01HL116577-01 to MRK2 and SIS; 1R35HL144976-01 to WB), and the University of North Carolina School of Medicine. MKK and RHL received funding through the UNC Hematology NIH T32 Training Grant (HL007149-42). EBP was supported by the American Heart Association Postdoctoral Fellowship Award 18POST33960499. SIS acknowledges funding from the Louis A. Simpson and Kimberly K. Querrey Center for Regenerative Nanomedicine at Northwestern University through a CRN Catalyst Award. The UNC Electron Microscopy Facility is supported in part by the Lineberger Comprehensive Cancer Center UCRF. Peptide amphiphile synthesis was performed in the Peptide Synthesis Core Facility of the Simpson Querrey Institute at Northwestern University. The U.S. Army Research Office, the U.S. Army Medical Research and Materiel Command, and Northwestern University provided funding to develop this facility and ongoing support is being received from the Soft and Hybrid Nanotechnology Experimental (SHyNE) Resource (NSF ECCS-1542205).

The authors would like to thank K. Wallace and D. Hepp for their administrative assistance with this manuscript. We would also like to thank the UNC Structural Biology Core for their assistance with the SBC-X PA nanofiber sequences. We gratefully acknowledge J. Griffith and S. Willcox in the Lineberger Cancer Center EM Core Facility for assistance with conventional TEM. Tristan D. Clemons graciously acknowledges support from an American Australian Association-Dow Chemical Company Scholarship. We acknowledge the following core facilities at Northwestern University: the Peptide Synthesis Core Facility and the Analytical BioNanoTechnology Equipment Core Facility (ANTEC) of the Simpson Querrey Institute for peptide synthesis and purification, and the Biological Imaging Facility (BIF) for cryo-TEM. X-ray scattering experiments were performed at the DuPont-Northwestern-Dow Collaborative Access Team (DND-CAT) located at Sector 5 of the Advanced Photon Source. DND-CAT is supported by E.I. DuPont de Nemours & Co., the Dow Chemical Company, and the State of Illinois. This research used resources of the Advanced Photon Source, a U.S. Department of Energy (DOE) Office of Science User Facility operated for the DOE Office of Science by Argonne National Laboratory under Contract No. DE-AC02-06CH11357. Cryo-TEM images made use of the BioCryo facility of Northwestern University's NUANCE Center, which has received support from the Soft and Hybrid Nanotechnology Experimental (SHyNE) Resource (NSF ECCS-1542205); the MRSEC program (NSFDMR-1720139) at the Materials Research Center; the International Institute for Nanotechnology (IIN); and the State of Illinois, through the IIN. The authors thank N.D. Riggsbee and T.C. Nichols for help and advice with thromboelastography (TEG). The views expressed in this article are those of the authors and do not necessarily reflect the official policy or position of the Air Force, the Department of Defense, or the U.S. Government; cleared, SAF/PA, Case #2019-0302, 24 Apr 2019.

References

1. Koh EY; Oyeniyi BT; Fox EE; Scerbo M; Tomasek JS; Wade CE; Holcomb JB, Trends in Potentially Preventable Trauma Deaths Between 2005–2006 and 2012–2013. Am J Surg 2019, 218, 501–506. [PubMed: 30595330]
2. Eastridge BJ; Mabry RL; Seguin P; Cantrell J; Tops T; Uribe P; Mallett O; Zubko T; Oetjen-Gerdes L; Rasmussen TE; Butler FK; Kotwal RS; Holcomb JB; Wade C; Champion H; Lawnick M; Moores L; Blackbourne LH, Death on the Battlefield (2001–2011): Implications for the Future of Combat Casualty Care. J Trauma Acute Care Surg 2012, 73, S431–437. [PubMed: 23192066]
3. Morrison JJ; Galgon RE; Jansen JO; Cannon JW; Rasmussen TE; Eliason JL, A Systematic Review of the Use of Resuscitative Endovascular Balloon Occlusion of the Aorta in the Management of Hemorrhagic Shock. J Trauma Acute Care Surg 2016, 80, 324–334. [PubMed: 26816219]
4. Manley JD; Mitchell BJ; DuBose JJ; Rasmussen TE, A Modern Case Series of Resuscitative Endovascular Balloon Occlusion of the Aorta (REBOA) in an Out-of-Hospital, Combat Casualty Care Setting. J Spec Oper Med 2017, 17, 1–8. [PubMed: 28285473]
5. Reva VA; Horer TM; Makhnovskiy AI; Sokhranov MV; Samokhvalov IM; DuBose JJ, Field and En Route Resuscitative Endovascular Occlusion of the Aorta: A Feasible Military Reality? J Trauma Acute Care Surg 2017, 83, S170–s176. [PubMed: 28628603]
6. Chang JC; Holloway BC; Zamisch M; Hepburn MJ; Ling GS, ResQFoam for the Treatment of Non-Compressible Hemorrhage on the Front Line. Mil Med 2015, 180, 932–933. [PubMed: 26327542]
7. Duggan M; Rago A; Sharma U; Zugates G; Freyman T; Busold R; Caulkins J; Pham Q; Chang Y; Mejaddam A; Beagle J; Velmahos G; deMoya M; Zukerberg L; Ng TF; King DR, Self-Expanding Polyurethane Polymer Improves Survival in a Model of Noncompressible Massive Abdominal Hemorrhage. J Trauma Acute Care Surg 2013, 74, 1462–1467. [PubMed: 23694873]

8. Rago A; Duggan MJ; Marini J; Beagle J; Velmahos G; De Moya MA; Sharma U; Hwabejire J; King DR, Self-Expanding Foam Improves Survival Following a Lethal, Exsanguinating Iliac Artery Injury. J Trauma Acute Care Surg 2014, 77, 73–77. [PubMed: 24977758]
9. Rago AP; Larentzakis A; Marini J; Picard A; Duggan MJ; Busold R; Helmick M; Zugates G; Beagle J; Sharma U; King DR, Efficacy of a Prehospital Self-Expanding Polyurethane Foam for Noncompressible Hemorrhage Under Extreme Operational Conditions. J Trauma Acute Care Surg 2015, 78, 324–329. [PubMed: 25757118]
10. Rago AP; Marini J; Duggan MJ; Beagle J; Runyan G; Sharma U; Peev M; King DR, Diagnosis and Deployment of a Self-Expanding Foam for Abdominal Exsanguination: Translational Questions for Human Use. J Trauma Acute Care Surg 2015, 78, 607–613. [PubMed: 25710434]
11. Shakur H; Roberts I; Bautista R; Caballero J; Coats T; Dewan Y; El-Sayed H; Gogichaishvili T; Gupta S; Herrera J; Hunt B; Iribhogbe P; Izurieta M; Khamis H; Komolafe E; Marrero MA; Mejia-Mantilla J; Miranda J; Morales C; Olaomi O, et al., Effects of Tranexamic Acid on Death, Vascular Occlusive Events, and Blood Transfusion in Trauma Patients with Significant Haemorrhage (CRASH-2): A Randomised, Placebo-Controlled Trial. Lancet 2010, 376, 23–32. [PubMed: 20554319]
12. Myers SP; Kutcher ME; Rosengart MR; Sperry JL; Peitzman AB; Brown JB; Neal MD, Tranexamic Acid Administration Is Associated with an Increased Risk of Posttraumatic Venous Thromboembolism. J Trauma Acute Care Surg 2019, 86, 20–27. [PubMed: 30239375]
13. Petersen LC; Valentin S; Hedner U, Regulation of the Extrinsic Pathway System in Health and Disease: The Role of Factor VIIa and Tissue Factor Pathway Inhibitor. Thromb Res 1995, 79, 1–47. [PubMed: 7495097]
14. Moyer TJ; Kassam HA; Bahnson ES; Morgan CE; Tantakitti F; Chew TL; Kibbe MR; Stupp SI, Shape-Dependent Targeting of Injured Blood Vessels by Peptide Amphiphile Supramolecular Nanostructures. Small 2015, 11, 2750–2755. [PubMed: 25649528]
15. Cui H; Webber MJ; Stupp SI, Self-Assembly of Peptide Amphiphiles: From Molecules to Nanostructures to Biomaterials. Biopolymers 2010, 94, 1–18. [PubMed: 20091874]
16. Aida T; Meijer EW; Stupp SI, Functional Supramolecular Polymers. Science 2012, 335, 813–817. [PubMed: 22344437]
17. Banner DW; D'Arcy A; Chene C; Winkler FK; Guha A; Konigsberg WH; Nemerson Y; Kirchhofer D, The Crystal Structure of the Complex of Blood Coagulation Factor VIIa with Soluble Tissue Factor. Nature 1996, 380, 41–46. [PubMed: 8598903]
18. Dickinson CD; Kelly CR; Ruf W, Identification of Surface Residues Mediating Tissue Factor Binding and Catalytic Function of the Serine Protease Factor VIIa. Proc Natl Acad Sci 1996, 93, 14379–14384. [PubMed: 8962059]
19. Song H; Olsen OH; Persson E; Rand KD, Sites Involved in Intra-and Interdomain Allostery Associated with the Activation of Factor VIIa Pinpointed by Hydrogen-Deuterium Exchange and Electron Transfer Dissociation Mass Spectrometry. J Biol Chem 2014, 289, 35388–35396. [PubMed: 25344622]
20. Hagen FS; Gray CL; O'Hara P; Grant FJ; Saari GC; Woodbury RG; Hart CE; Insley M; Kisiel W; Kurachi K; Davie EW, Characterization of a cDNA Coding for Human Factor VII. Proc Natl Acad Sci U S A 1986, 83, 2412–2416. [PubMed: 3486420]
21. Morgan CE; Dombrowski AW; Rubert Perez CM; Bahnson ES; Tsihlis ND; Jiang W; Jiang Q; Vercammen JM; Prakash VS; Pritts TA; Stupp SI; Kibbe MR, Tissue-Factor Targeted Peptide Amphiphile Nanofibers as an Injectable Therapy to Control Hemorrhage. ACS Nano 2016, 10, 899–909. [PubMed: 26700464]
22. Cui H; Cheetham AG; Pashuck ET; Stupp SI, Amino Acid Sequence in Constitutionally Isomeric Tetrapeptide Amphiphiles Dictates Architecture of One-Dimensional Nanostructures. J Am Chem Soc 2014, 136, 12461–12468. [PubMed: 25144245]
23. Tantakitti F; Boekhoven J; Wang X; Kazantsev RV; Yu T; Li J; Zhuang E; Zandi R; Ortony JH; Newcomb CJ; Palmer LC; Shekhawat GS; Olvera de la Cruz M; Schatz GC; Stupp SI, Energy Landscapes and Functions of Supramolecular Systems. Nat Mater 2016, 15, 469–476. [PubMed: 26779883]

24. Sato K; Ji W; Alvarez Z; Palmer LC; Stupp SI, Chiral Recognition of Lipid Bilayer Membranes by Supramolecular Assemblies of Peptide Amphiphiles. ACS Biomater Sci Eng 2019, 5, 2786–2792.
25. Greenfield NJ, Using Circular Dichroism Spectra to Estimate Protein Secondary Structure. Nat Protoc 2006, 1, 2876–2890. [PubMed: 17406547]
26. Bahnson ES; Kassam HA; Moyer TJ; Jiang W; Morgan CE; Vercammen JM; Jiang Q; Flynn ME; Stupp SI; Kibbe MR, Targeted Nitric Oxide Delivery by Supramolecular Nanofibers for the Prevention of Restenosis After Arterial Injury. Antioxid Redox Signal 2016, 24, 401–418. [PubMed: 26593400]
27. Estcourt LJ; Desborough M; Brunskill SJ; Doree C; Hopewell S; Murphy MF; Stanworth SJ, Antifibrinolytics (Lysine Analogues) for the Prevention of Bleeding in People with Haematological Disorders. Cochrane Database Syst Rev 2016, 3, Cd009733. [PubMed: 26978005]
28. Stettler GR; Moore EE; Moore HB; Lawson PJ; Fragoso M; Nunns GR; Silliman CC; Banerjee A, Thrombelastography Indicates Limitations of Animal Models of Trauma-Induced Coagulopathy. J Surg Res 2017, 217, 207–212. [PubMed: 28583756]
29. Mann KG; Whelihan MF; Butenas S; Orfeo T, Citrate Anticoagulation and the Dynamics of Thrombin Generation. J Thromb Haemost 2007, 5, 2055–2061. [PubMed: 17883701]
30. Getz T; Piatt R; Petrich B; Monroe D; Mackman N; Bergmeier W, Novel Mouse Hemostasis Model for Real-Time Determination of Bleeding Time and Hemostatic Plug Composition. J Thromb Haemostasis 2015, 13, 417–425. [PubMed: 25442192]
31. Bertram JP; Williams CA; Robinson R; Segal SS; Flynn NT; Lavik EB, Intravenous Hemostat: Nanotechnology to Halt Bleeding. Sci Transl Med 2009, 1, 11ra22.
32. Shoffstall AJ; Atkins KT; Groynom RE; Varley ME; Everhart LM; Lashof-Sullivan MM; Martyn-Dow B; Butler RS; Ustin JS; Lavik EB, Intravenous Hemostatic Nanoparticles Increase Survival Following Blunt Trauma Injury. Biomacromolecules 2012, 13, 3850–3857. [PubMed: 22998772]
33. Shoffstall AJ; Everhart LM; Varley ME; Soehnlen ES; Shick AM; Ustin JS; Lavik EB, Tuning Ligand Density on Intravenous Hemostatic Nanoparticles Dramatically Increases Survival Following Blunt Trauma. Biomacromolecules 2013, 14, 2790–2797. [PubMed: 23841817]
34. Cheng J; Feng S; Han S; Zhang X; Chen Y; Zhou X; Wang R; Li X; Hu H; Zhang J, Facile Assembly of Cost-Effective and Locally Applicable or Injectable Nanohemostats for Hemorrhage Control. ACS Nano 2016, 10, 9957–9973. [PubMed: 27736084]
35. Shukla M; Sekhon UD; Betapudi V; Li W; Hickman DA; Pawlowski CL; Dyer MR; Neal MD; McCrae KR; Sen Gupta A, *In Vitro* Characterization of Synthoplate (Synthetic Platelet) Technology and Its In Vivo Evaluation in Severely Thrombocytopenic Mice. J Thromb Haemost 2017, 15, 375–387. [PubMed: 27925685]
36. Dyer M; Haldeman S; Gutierrez A; Kohut L; Sen Gupta A; Neal MD, Uncontrolled Hemorrhagic Shock Modeled Via Liver Laceration in Mice with Real Time Hemodynamic Monitoring. J Vis Exp 2017.
37. Chan LW; Wang X; Wei H; Pozzo LD; White NJ; Pun SH, A Synthetic Fibrin Cross-Linking Polymer for Modulating Clot Properties and Inducing Hemostasis. Sci Transl Med 2015, 7, 277ra229.
38. Letson HL; Dobson GP, Correction of Acute Traumatic Coagulopathy with Small-Volume 7.5% NaCl Adenosine, Lidocaine, and Mg2+ Occurs Within 5 Minutes: A ROTEM Analysis. J Trauma Acute Care Surg 2015, 78, 773–783. [PubMed: 25807406]
39. Letson HL; Dobson GP, 3.0% NaCl Adenosine, Lidocaine, Mg 2+ (ALM) Bolus and 4 Hours 'Drip' Infusion Reduces Non-Compressible Hemorrhage by 60% in a Rat Model. J Trauma Acute Care Surg 2017.
40. Ilavsky J; Jemian PR, Irena: Tool Suite for Modeling and Analysis of Small-Angle Scattering. J Appl Crystallogr 2009, 42, 347–353.
41. Morgan CE; Prakash VS; Vercammen JM; Pritts T; Kibbe MR, Development and Validation of 4 Different Rat Models of Uncontrolled Hemorrhage. JAMA Surgery 2015, 150, 316–324. [PubMed: 25693160]

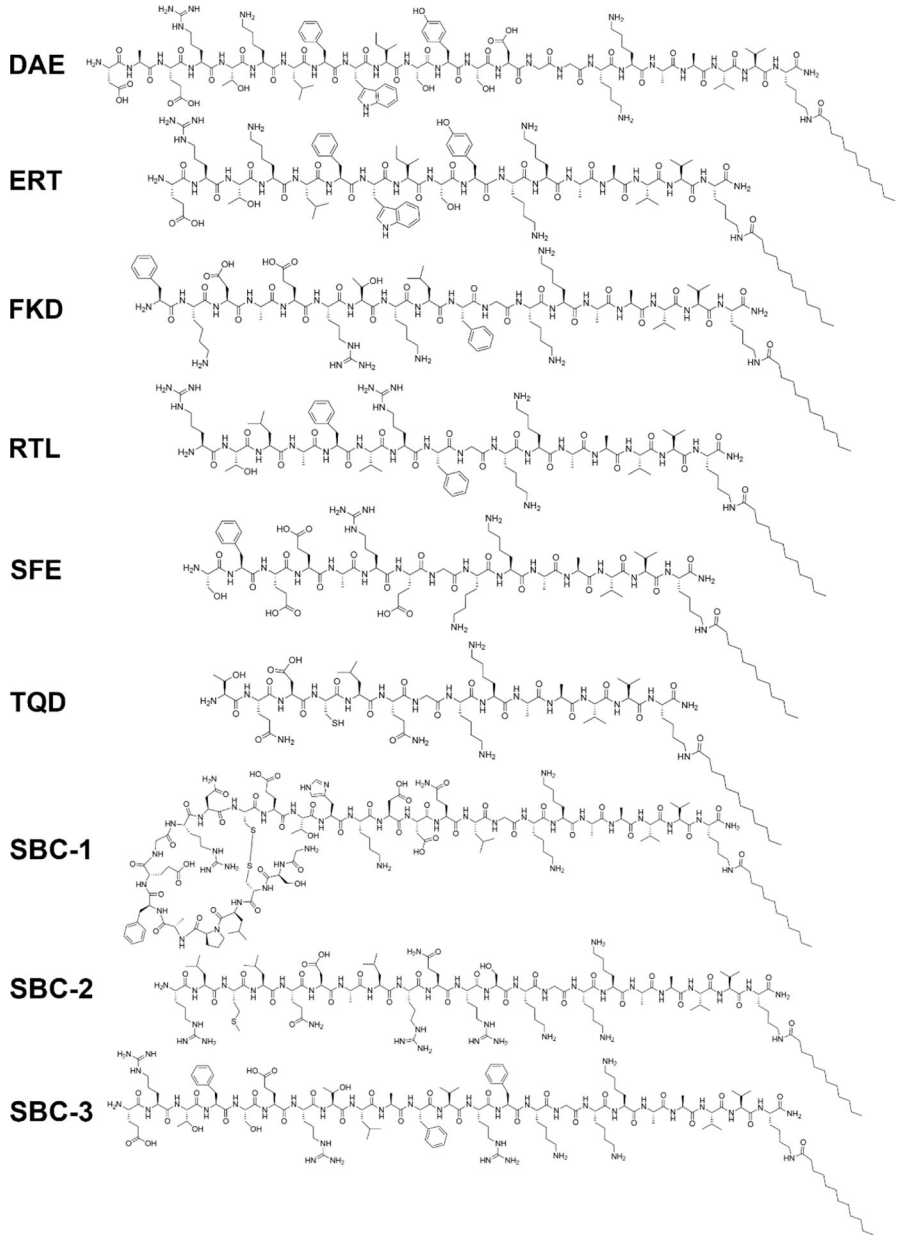

Figure 1.

Chemical structures of the FVII-derived TF-targeting peptide amphiphiles with their three-letter abbreviations shown on the left. The Structural Biology Core at UNC generated three TF-targeting sequences (SBC-X) based on interactions observed in the TF-FVII crystal structure, with amino acid substitutions to enhance α-helix formation and improve targeting.

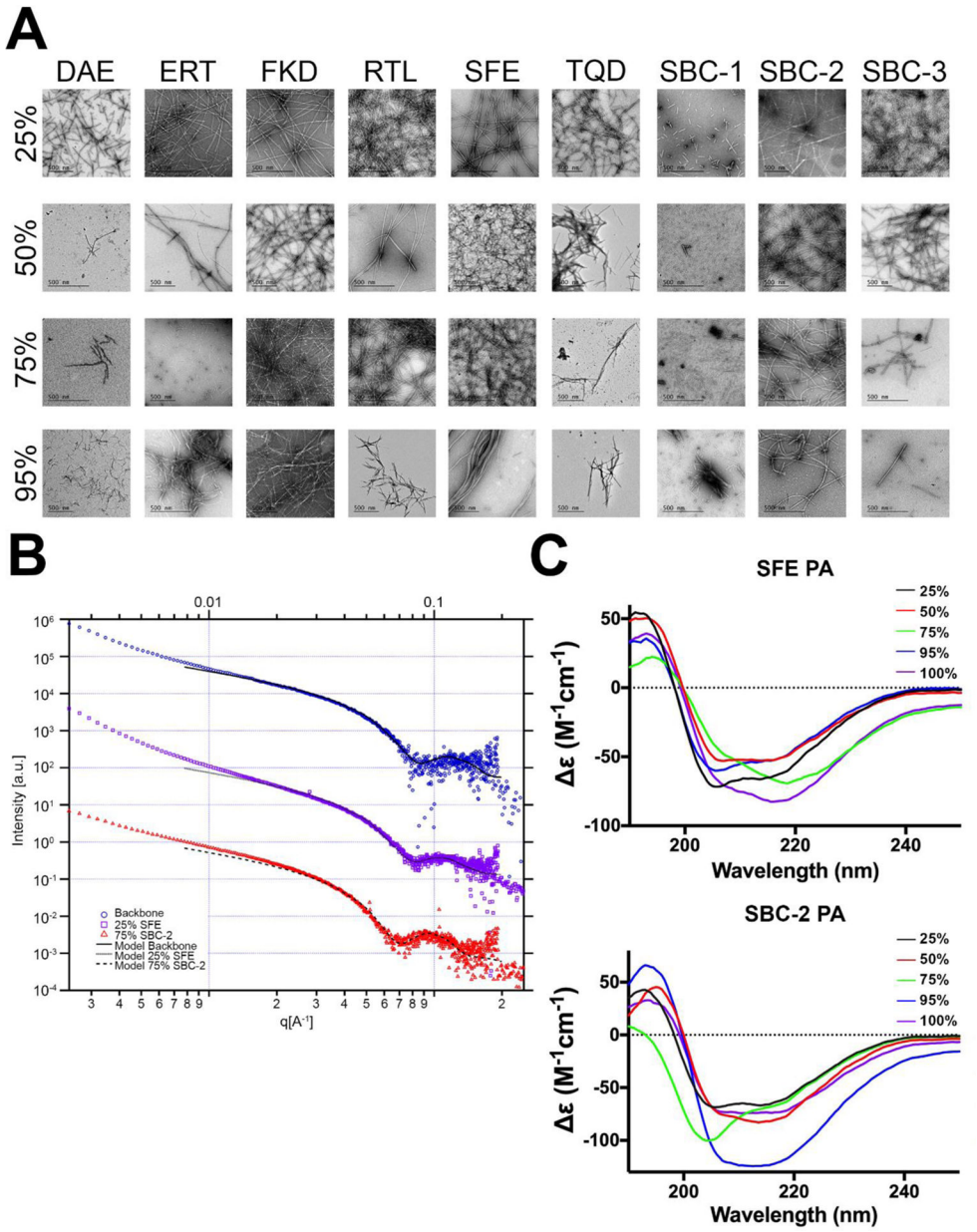

Figure 2.

Characterization of TF-targeted nanofibers. (**A**) Transmission electron micrographs of TF-targeted nanofibers co-assembled at ratios of 25, 50, 75, and 95% TF-targeting sequence, with the remaining percent being KKAAVV-K(*N*-ε-lauroyl) backbone PA nanofiber. (**B**) Solution-phase small-angle X-ray scattering of the backbone alone, with 25% SFE, or with 75% SBC-2 PA. (**C**) Circular dichroism spectroscopy of the SFE PA and SBC-2 PA, showing α-helical characteristics in addition to the expected β-sheet conformation.

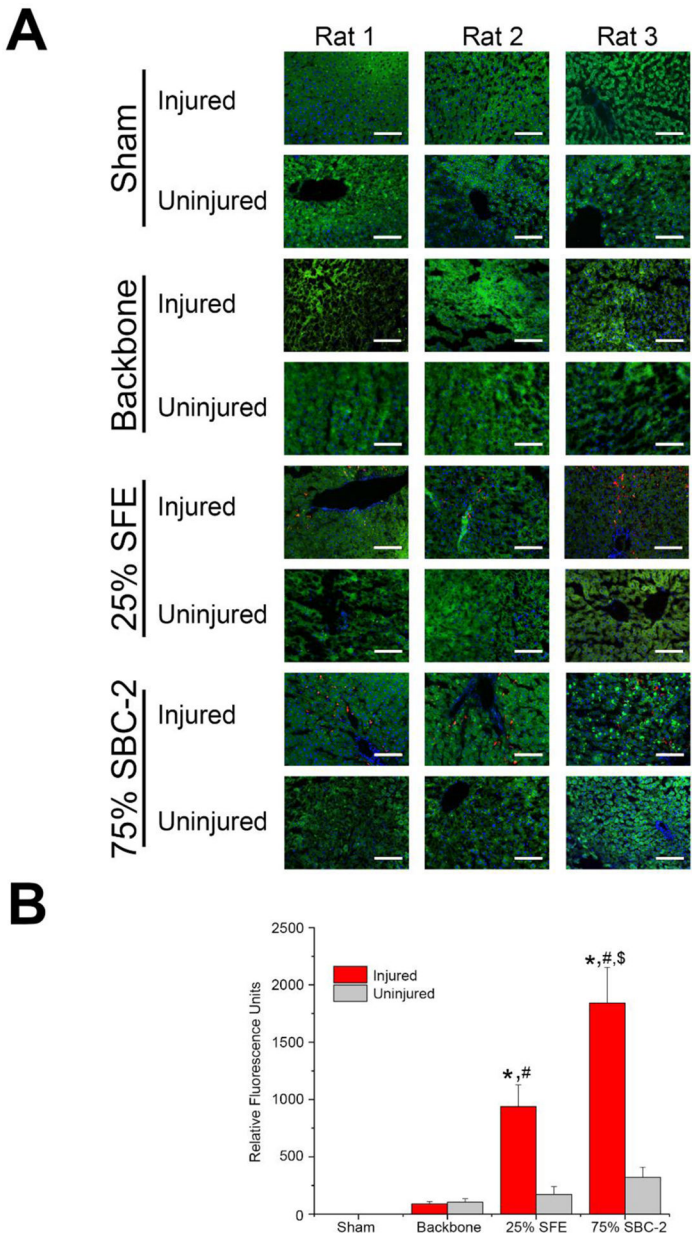

Figure 3.

SFE and SBC-2 PA nanofibers localize to areas of non-compressible liver injury in a rat hemorrhage model *in vivo*. (**A**) Fluorescence microscopy of injured and uninjured livers demonstrates localization of the 25% SFE PA nanofiber and 75% SBC-2 PA nanofiber to sites of liver injury with minimal signal in the uninjured liver. Blue = DAPI nuclear stain, green = autofluorescence of liver, and red = TAMRA-tagged nanofiber, scale bar=100 μm; n=6/treatment group. (**B**) Quantification of fluorescence demonstrates the highest fluorescence in the injured liver with 75% SBC-2 PA nanofiber. $^{*}p < 0.05$ injured *versus* uninjured liver fluorescence; $^{\#}p < 0.05$ injured SFE PA nanofiber and injured SBC-2 PA nanofiber treatment group compared to injured backbone PA nanofiber treatment group; $^{\$}p <$

0.05 injured liver from animals given SBC-2 PA nanofiber compared to injured livers from animals given SFE PA nanofiber.

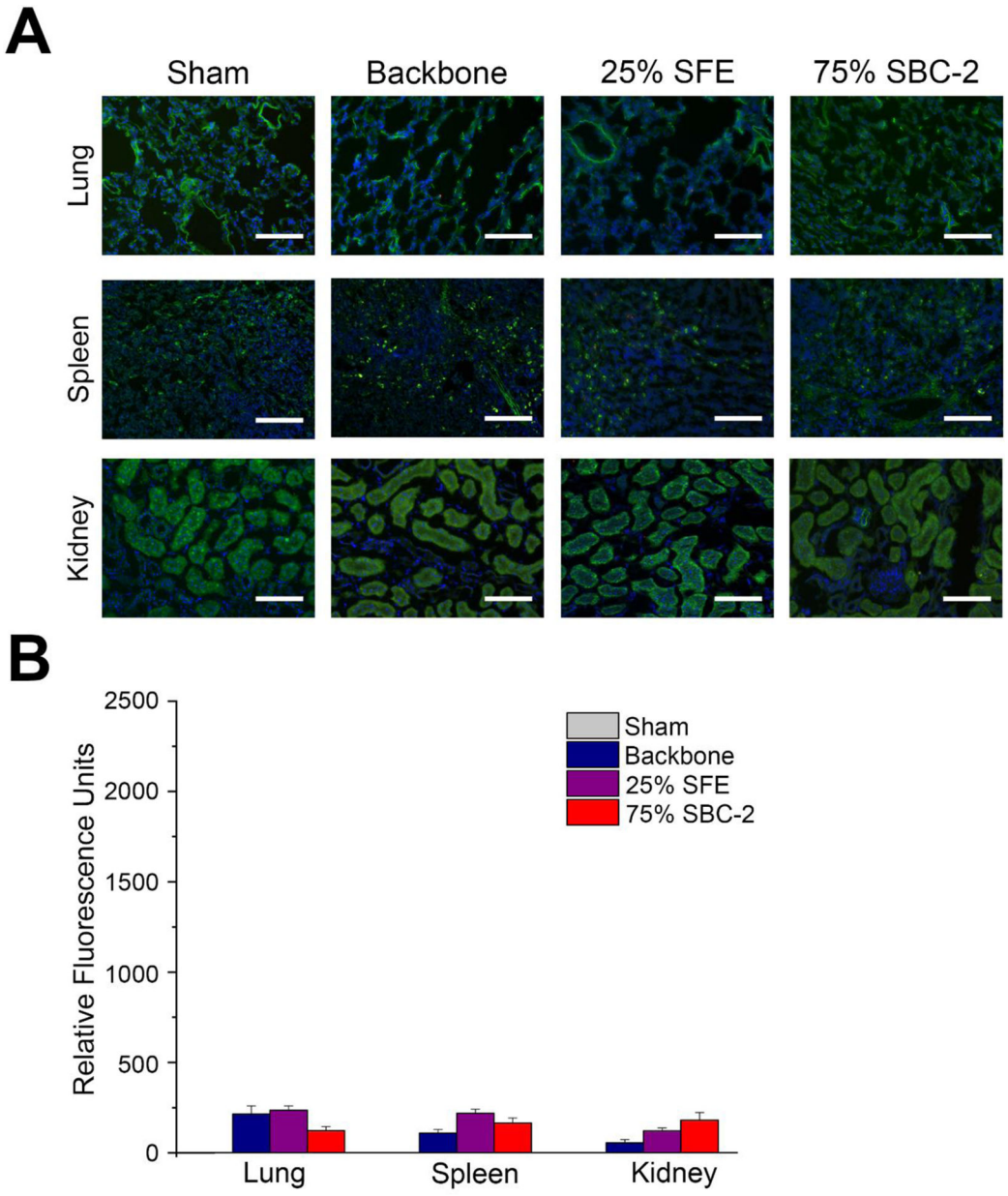

Figure 4.

SFE and SBC-2 PA nanofibers show minimal off-target localization. Uninjured lung, spleen, and kidney show little fluorescence (**A**), with no difference seen in SFE PA and SBC-2 PA nanofibers compared to backbone PA nanofiber alone in animals that underwent liver hemorrhage model (**B**). Blue = DAPI nuclear stain, green = autofluorescence of the tissue, red = TAMRA-tagged nanofiber; scale bar=100 μm; n=3/treatment group.

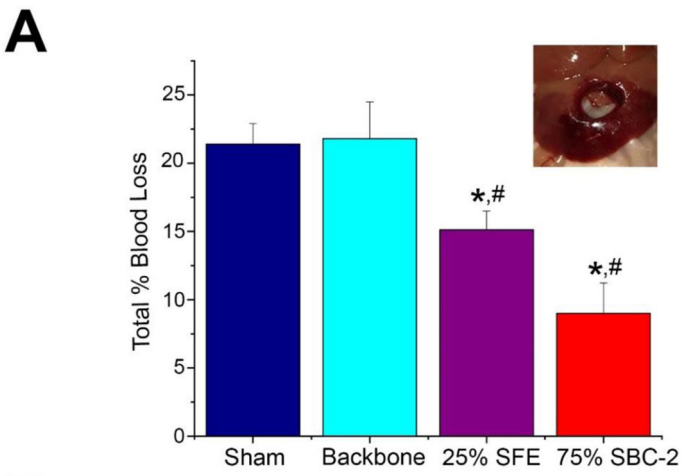

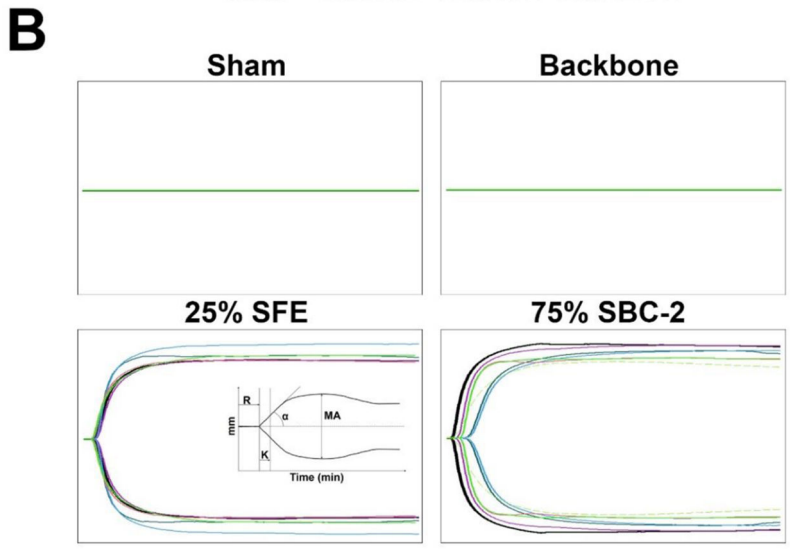

C

Treatment	Dose	R time (min)	K time (min)	MA (mm)	LY30 (%)
Sham	100 µL	-	-	-	-
Backbone	0.2 µg	-	-	-	-
25% SFE	0.2 µg	2.23 (1.8-2.6)	1.03 (0.8-1.2)	74.58 (72.0-77.8)	0 (0)
75% SBC-2	0.2 µg	3.05 (2.0-4.4)	1.22 (0.9-1.8)	65.12 (59.5-71.0)	0 (0)

Figure 5.

25% SFE PA and 75% SBC-2 PA nanofibers decrease blood loss compared to sham animals in a liver hemorrhage model, and initiate clotting in anti-coagulated blood. (**A**) Assessment of % total blood loss in a central liver punch injury caused by a 12-mm punch biopsy (*inset*) and used to model non-compressible hemorrhage revealed less blood loss with 25% SFE PA and 75% SBC-2 PA nanofiber treatment groups compared to sham ($^{*}p < 0.05$) and backbone PA nanofiber controls ($^{\#}p < 0.05$); n=6/ treatment group. (**B**) Superimposed TEG curves from n=6 animals in anti-coagulated rat blood. 25% SFE PA and 75% SBC-2 PA nanofiber treatment groups initiate clotting in the presence of human TF despite anti-coagulation with heparin, with no clotting (indicated by flat line) seen in controls. Green lines in controls indicate overlapping curves. Inset shows axis labels and parameter origins. Experiments

were run for at least 60 min and up to 120 min (X-axis). (**C**) R time (reaction time, measures how fast blood clots), K time (kinetic time, measures how fast a clot reaches a specific strength), MA (maximum amplitude, highest clot strength), and LY30 (lysis 30 min after MA, measures how stable the clot is) from TEG curves, with (−) in controls indicating no clotting was observed, therefore the relevant numbers could not be generated.

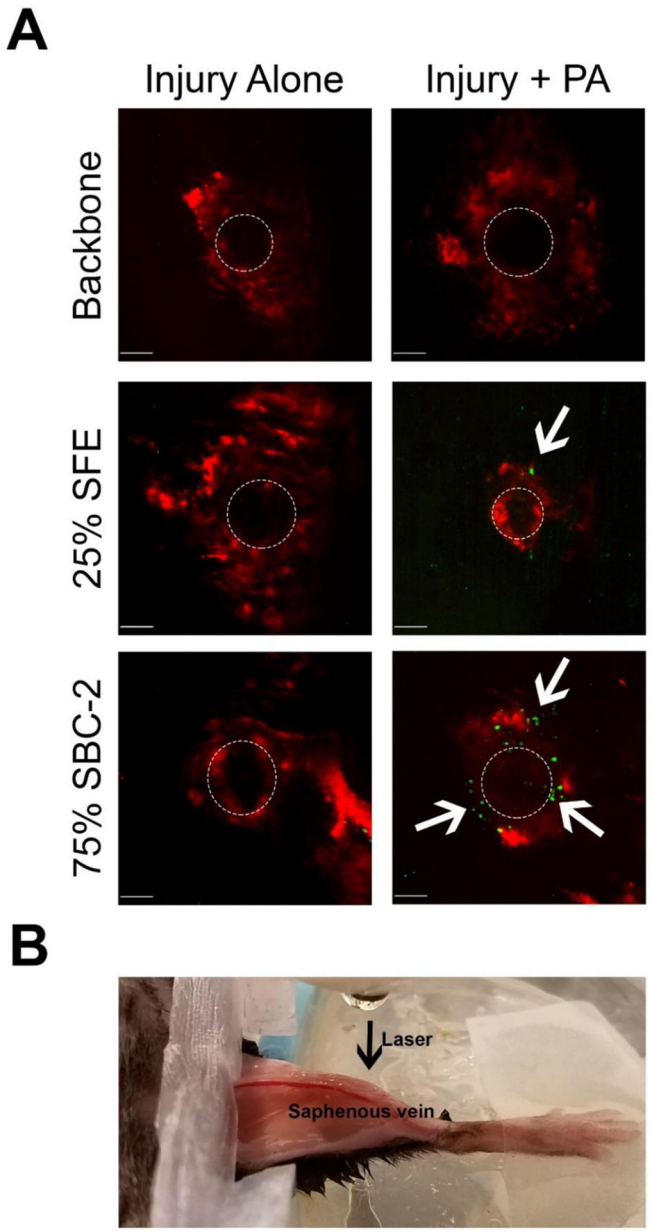

Figure 6.

SFE and SBC-2 PA nanofibers localize to sites of TF expression in a mouse vein laser injury model *in vivo*. (**A**) Confocal Z-stacks of hemostatic plugs show that SFE and SBC-2 PA nanofibers (green fluorescence, white arrows) co-localize with fibrin (red) at the site of laser injury (white dashed circle). (**B**) Mouse positioning and saphenous vein exposure prior to injury. The black arrow indicates the direction of laser injury (perpendicular to the blood vessel). Scale bar=25 μm; n=3/treatment group.